



In-situ nano-alloying Pd-Ni for economical control of syngas production from high-temperature thermo-electrochemical reduction of steam/CO₂



Si-Won Kim ^{a,b}, Mansoo Park ^a, Hyoungchul Kim ^a, Kyung Joong Yoon ^a, Ji-Won Son ^a, Jong-Ho Lee ^a, Byung-Kook Kim ^a, Jong-Heun Lee ^b, Jongsup Hong ^{a,*}

^a High Temperature Energy Materials Research Center, Korea Institute of Science and Technology, Hwarangno 14-gil 5, Seongbuk-gu, Seoul 136-791, South Korea

^b Department of Materials Science and Engineering, Korea University, Anam-dong, Seongbuk-gu, Seoul 136-713, South Korea

ARTICLE INFO

Article history:

Received 19 April 2016

Received in revised form 2 July 2016

Accepted 14 July 2016

Available online 15 July 2016

Keywords:

CO₂ reduction

Syngas production

Energy storage

Reverse water gas shift

Noble metal alloys

ABSTRACT

Developing high-density energy storage and lowering CO₂ emissions have been considered as key issues in energy and environmental science. To tackle these issues simultaneously, syngas production from high-temperature thermo-electrochemical reduction of steam/CO₂ mixtures utilizing renewable energy has been proposed. By doing so, renewable electrical energy can be stored in the form of chemical energy, and CO₂ is converted to highly valuable syngas which can be processed further to produce liquid fuels. To make this technology viable, it is imperative to develop a cost-effective and efficient methodology for controlling syngas production given that this system is linked with fluctuating renewable electrical current and CO₂ stream. Here we show that *in-situ* nano-alloying noble metals in solid oxide cells can provide such function by using substantially small amount of the expensive noble metals. Catalyzing selectively the reverse water gas shift reaction, this technique enables increasing the CO₂ conversion rate, storing energy more efficiently, and controlling the syngas production rate and its quality. Consequently, it may enhance the syngas productivity and energy storage capacity and provide a capability for adjusting effectively the system to variable renewable electrical energy and CO₂ sources.

© 2016 Elsevier B.V. All rights reserved.

1. Introduction

High-temperature thermo-electrochemical reduction of steam/CO₂ mixtures has been proposed as a potential solution to reduce CO₂ emissions and alleviate power fluctuation of renewable energy sources. Conventional solid oxide cells have been used to perform such functions converting steam/CO₂ mixtures to syngas and storing renewable electrical energy in the form of chemical energy. The produced syngas, comprised with H₂ and CO, can be post-processed by chemical synthesis such as the Fischer-Tropsch process to produce synthetic fuels [1–6]. When these cells are connected with renewable energy and CO₂ sources, their variable electrical current and gas flow rates, respectively, may affect significantly the internal reacting environment, especially inside fuel-electrodes. In their fuel-electrodes, oxygen ion conduction and the presence of carbon-containing species with steam form a

complex reacting environment where thermochemical reactions, *i.e.*, reverse water gas shift (RWGS), are coupled with electrochemical processes, *i.e.*, H₂O and CO₂ electrolysis (see Supplementary Table S1). Given the coupled endothermic processes, the extent of each reaction determines the overall energy requirements and products compositions (*i.e.*, H₂/CO ratio) that subsequently influence post-processing of the produced syngas. Consequently, the fuel-electrodes need to accommodate the various operating conditions while delivering the syngas with sufficient production yield and desirable compositions. The control of syngas production through the extent of each reaction and operating current and voltage is imperative to deliver syngas with sufficient yield and desirable compositions while storing electrical energy effectively and efficiently [7], which can be achieved by employing advanced fuel-electrode materials and its microstructure.

A nanoalloy-assisted production control technique is a promising methodology to provide the capability of controlling syngas production economically and sufficient performance for thermo-electrochemical reduction of steam/CO₂ mixtures. Previous studies showed that H₂O electrolysis is a primary reaction in conventional

* Corresponding author.

E-mail addresses: jhong@kist.re.kr, jongsup.hong@gmail.com (J. Hong).

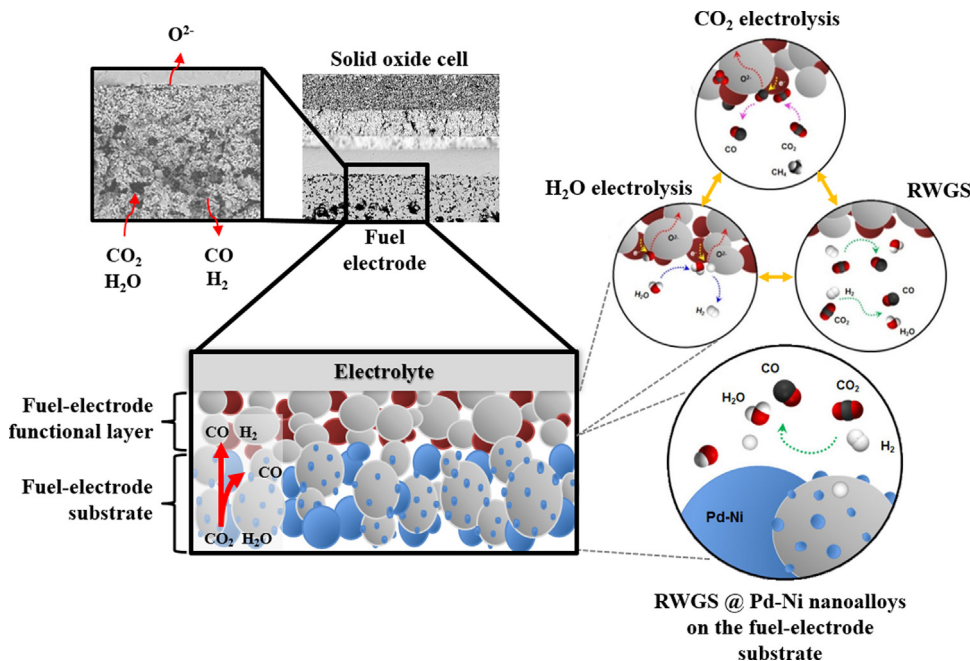


Fig. 1. Principles of *in-situ* nano-alloying Pd-Ni for the control of syngas production from high-temperature thermo-electrochemical reduction of steam/CO₂ mixtures. Pd-Ni nanoalloys are established only on the fuel-electrode substrate where thermochemical reactions predominantly take place, as compared to the fuel-electrode functional layer in which electrochemical reactions primarily proceed, which enhances CO₂ conversion by catalyzing the reverse water gas shift (RWGS) reaction.

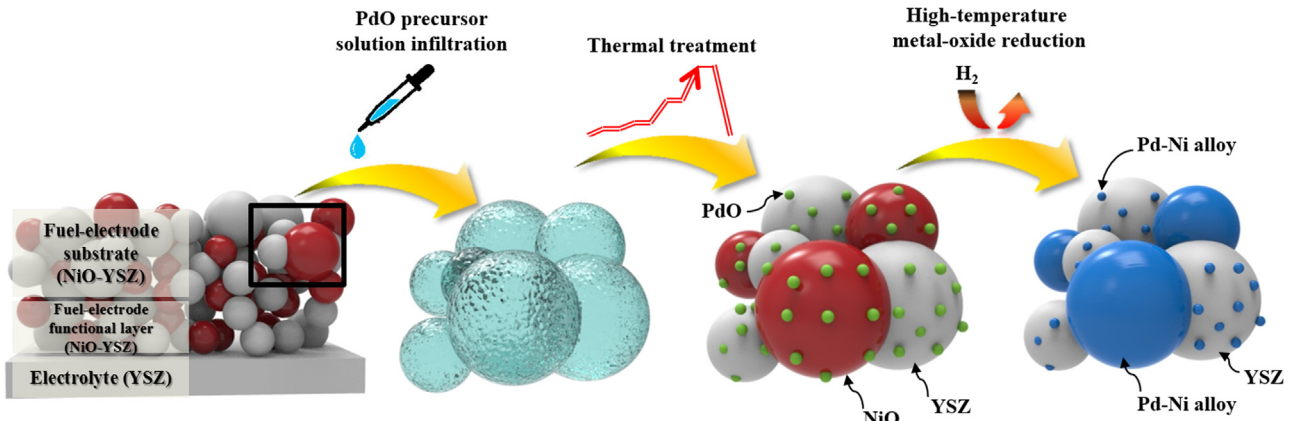


Fig. 2. Development of *in-situ* nano-alloyed Pd-Ni, established uniformly throughout the fuel-electrode substrate, by an advanced infiltration technique facilitating homogeneous nucleation of metal-oxide nanoparticles anchored on the NiO/YSZ backbone structure and the subsequent *in-situ* alloying Pd and Ni by the high-temperature metal-oxide reduction process using wet hydrogen.

fuel-electrodes, and such electrodes show insufficient catalysis for CO₂ reduction, which is predominantly governed by the RWGS reaction [8–14]. To control syngas production and enhance CO-selectivity, it has been discussed that lowering the activation energy for CO₂ reduction is necessary. This can be implemented by anchoring and nano-alloying noble metal catalysts such as Pd on the Ni/YSZ fuel-electrode substrate where the thermochemical reactions such as the RWGS reaction proceeds dominantly, as illustrated in Fig. 1. Pd has been shown to exhibit excellent catalytic performance for the RWGS reaction and stability in CO₂-flowing environments [15–21], and its catalytic activity is further enhanced by forming Pd-Ni alloys [22–25]. Other potential catalysts that can be used for the same objective include Fe, Co, Rh and Ru [26,27]. However, application of the precious metal is so expensive that its amount used needs to be minimized while providing sufficient catalytic performance. To meet these needs, in this study, an advanced infiltration technique facilitating homogeneous nano-catalysts nucleation and superior wetting was employed, followed

by thermal treatment to proceed *in-situ* nano-alloying impregnated Pd nanoparticles with Ni, as shown in Fig. 2. This enables uniform formation of Pd-Ni nanoalloys in the fuel-electrode substrate using substantially small amount of Pd loadings. With an aid of such uniform *in-situ* nano-alloying technique, a solid oxide cell supported by the nano-structured fuel-electrode substrate including uniformly distributed Pd-Ni nanoalloys was successfully fabricated, which enables increasing the CO₂ conversion rate, operating the cell at a higher current density and controlling the syngas production rate.

2. Experimental

The solid oxide cells used in this study are planar and fuel electrode-supported, which are comprised of a Ni-yttria-stabilized zirconia (YSZ) substrate, Ni-YSZ fuel-electrode functional layer, YSZ electrolyte, gadolinium-doped ceria (GDC) interdiffusion barrier layer, lanthanum-strontium-cobalt (LSC)-GDC air-electrode

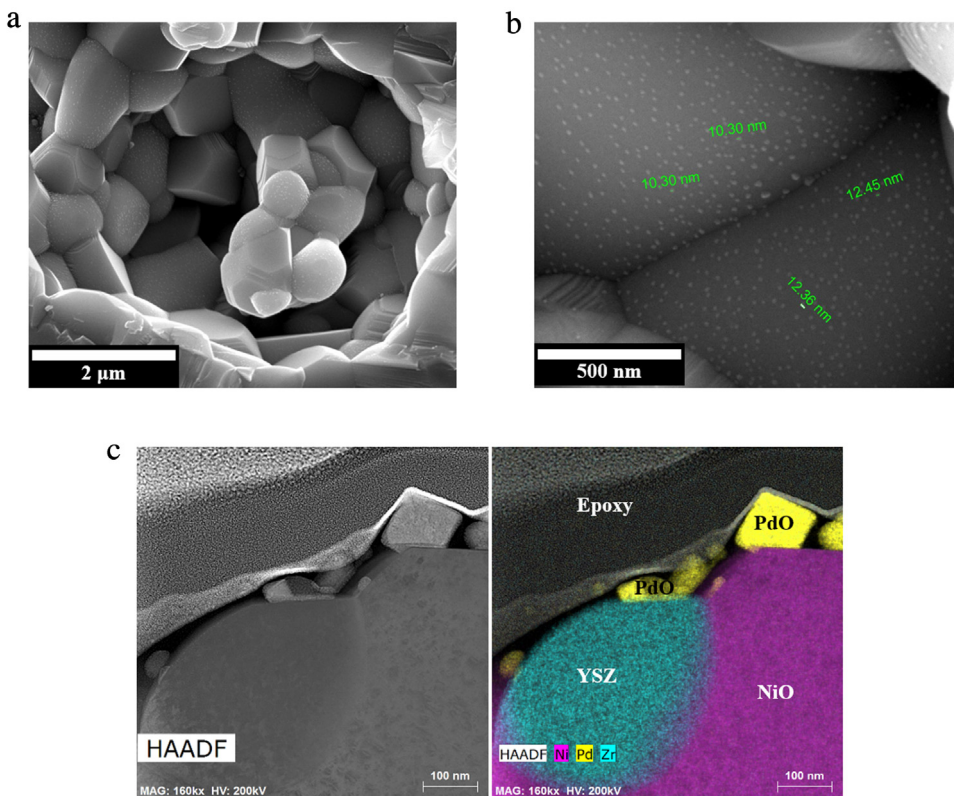


Fig. 3. PdO nanoparticles anchored on the NiO/YSZ fuel-electrode substrate: (a) SEM image showing the uniform distribution of the PdO nanoparticles throughout the fuel-electrode substrate; (b) SEM image highlighting the homogeneous morphology of the PdO nanoparticles and their size in the range of ten nanometers; (c) TEM image with EDS analysis results identifying PdO, NiO and YSZ particles and elucidating that the PdO nanoparticles are anchored on both NiO and YSZ particles in the fuel-electrode substrate. Mounting materials such as epoxy are seen on top of the NiO, PdO and YSZ particles.

functional layer and LSC air-electrode current collection layer. For fabrication of the fuel-electrode substrate, NiO (Sumitomo Metal Mining, Japan), YSZ (8 mol% Y_2O_3 stabilized ZrO_2 (TZ-8Y), Tosoh Corp., Japan) and a poly(methyl methacrylate)(PMMA) pore-forming agent was mixed with dispersant (HypermerTM KD-6, Croda, United Kingdom), binder (ethyl cellulose, Sigma-Aldrich, USA) and plasticizer (dibutyl phthalate, Junsei chemical, Japan) in ethanol and ball-milled for 24 h. The volume ratio between NiO, YSZ and PMMA is 0.37:0.33:0.3. NiO-YSZ composite granules were obtained by spray drying, which were subsequently compacted by uni-axial pressing at 60 MPa. The pastes for the fuel-electrode functional layers, electrolyte, interdiffusion barrier layer, air-electrode functional layers, and air-electrode current collecting layers were prepared by mixing corresponding powders with the dispersant, binder and plasticizer in solvent (α -terpineol, Kanto chemical, Japan) and using a planetary mill. The fuel-electrode functional layers and electrolyte were screen-printed on the substrate and co-sintered at 1400 °C. The interdiffusion barrier layer was screen-printed on top of the YSZ electrolyte and sintered at 1250 °C. Subsequently, the air-electrode functional layers and air-electrode current collecting layers were screen-printed and sintered at 950 °C. The size of the unit cells is 2 cm × 2 cm, and the effective electrode area is 1 cm × 1 cm.

Pd-Ni nanoalloys in the fuel-electrode substrate were fabricated by two consecutive steps such as PdO nanoparticles infiltration and *in-situ* nano-alloying through high-temperature metal-oxide reduction process. First, PdO nanoparticles were infiltrated to the porous fuel-electrode substrate by using their precursor solution mixed with urea and ethanol. To remove trapped air inside the fabricated unit cells, they were thermally treated at 400 °C for an hour prior to impregnation of PdO nanoparticles. The 0.3 mol L⁻¹

PdO precursor solution (tetraamminepalladium(II) nitrate solution [$\text{Pd}(\text{NH}_3)_4(\text{NO}_3)_2$], Sigma-Aldrich, USA) was mixed with urea (Sigma-Aldrich, USA) in a mixture of water and ethanol, which results in the molar ratio of urea to cation at 10 and the volume ratio of water to ethanol at 1.7. For desirable nanoparticles deposition, Lee et al. suggested the optimized [urea]/[cation] molar ratio of 10 and [water]/[ethanol] volume ratio of 1.7 [28], which was employed in this study. Infiltration was performed by applying the formulated solution to the fuel-electrode substrate surface. The infiltrated cells were thermally treated at 80 °C for 2 h to decompose urea, followed by secondary thermal treatment at 400 °C for an hour to remove organic compounds. The infiltration and thermal treatment steps were repeated 3 times prior to *in-situ* crystallization at 800 °C during cell operation. The amount of impregnated PdO nanoparticles was controlled by the weight change of the infiltrated cells measured by an analytical balance (XS204, Mettler Toledo, USA). The impregnated PdO nanoparticles as well as NiO embedded in the fuel-electrode substrate were reduced at 800 °C to Pd and Ni by using 10% wet H₂ (3% H₂O included) with the remainder being nitrogen. The resulting metals were subsequently nano-alloyed at the same temperature. The crystallization behavior of PdO nanoparticles and their chemical compatibility with NiO/YSZ were examined in a separate experiment by dispersing the NiO/YSZ powder in the PdO precursor solution, thermally treating it at 80 °C for 2 h and 800 °C for an hour, and characterizing the crystal structure of the resulting powder by using X-ray diffraction (XRD) (D8 Advance-Lynxeye, Bruker, USA).

The catalytic effect of Pd-Ni nanoalloys on CO₂ conversion, syngas production and electrochemical cell performance was investigated by using a solid oxide cell testing system which is detailed in [7]. The cells were heated within an electric furnace.

Hermetic sealing condition was obtained by using gasket-type composite sealants containing binary ceramic fillers within the glass matrix [29]. Cell voltage was measured by using potential probes welded to Inconel-based metallic end-plates. Current collection was enhanced by employing Ni foam and Pt mesh in between the end-plates and the fuel-electrode and the air-electrode, respectively. The total gas flow rates were maintained at 100 sccm and 200 sccm for the fuel and air electrode, respectively. The steam concentration in the fuel flow was controlled by a humidifier equipped with the reverse osmosis system (RO-Pure Plus, Premier, USA). The products gas composition was measured continuously by using online mass spectrometer (Hiden HPR-20 QIC, USA) and gas chromatography (Agilent 7890B, USA), both of which are connected to the tail-end of the cell-testing system. The microstructure of the cells was examined by using a scanning transmission electron microscope (S-TEM) (Talos F200X, FEI, USA) equipped with an energy-dispersed X-ray analyzer and a field emission scanning electron microscope (FE-SEM) (Inspect F50, FEI, USA).

3. Results and discussion

3.1. In-situ nano-alloyed Pd-Ni in the fuel-electrode substrate

In the development of the *in-situ* nano-structured fuel-electrode, it is crucial to obtain the uniformity of metal nano-catalysts distribution on the backbone structure and their alloying with the base-metal in the backbone at the cell operating temperature. These two requirements were achieved by metal-oxide infiltration based on a urea decomposition method and dual-solvent technique and subsequent high-temperature metal-oxide reduction procedure.

Given that Pd needs to be deposited on the thick fuel-electrode substrate having a low porosity of 22% (see Supplementary Fig. S1) by infiltration, it would be very difficult to impregnate its concentrated precursor solution uniformly into micro- and nano-pores of the porous scaffold by capillary force even under the vacuum treatment [30]. Since conventional infiltration techniques may not be sufficient for uniform nanoparticle distribution [31], an advanced impregnation process adding urea as a complexing/precipitating agent and ethanol as a co-solvent along with water was implemented in this study. Utilizing this novel process, the uniformity of PdO nanoparticles anchored on the entire NiO/YSZ substrate is obtained, as shown in Fig. 3. Note that PdO is reduced to Pd during the subsequent fuel-electrode reduction process using wet H₂ [32]. The size of impregnated PdO is on the order of 10 nm, and its particle morphology is homogeneous. The TEM image with EDS analysis shows that PdO nanoparticles are anchored on both NiO and YSZ grains. Nano-catalysts nucleation and precipitation from their precursor solution are controlled by the supply of ligand and which makes the cation solution exceed its solubility limit. In conventional infiltration methods, the ligand is added initially to the precursor solution, which cannot sustain its uniform supply during nano-catalysts precipitation. On the other hand, in the urea decomposition technique, urea pre-mixed in the precursor solution decomposes slowly to ammonia and CO₂ upon heating to 80 °C, providing uniformly the ligand (OH⁻ and CO₃²⁻ ions) throughout the solution and increasing its pH level [33]. The uniform supply of the ligand induces homogeneous nucleation and precipitation of metal hydroxides and hydroxycarbonates that are converted to PdO nanoparticles in the following calcination process. Since urea decomposition proceeds at temperature below the boiling point of the solvent, the uniform supply of the ligand proceeds throughout the precursor solution, improving the particle homogeneity. The uniformity of anchored PdO nanoparticles on the backbone

is further enhanced by improving the wetting property of aqueous solution. The lower surface tension of ethanol (22.3 mN m⁻¹ at 25 °C), in comparison with that of water (72.0 mN m⁻¹ at 25 °C), induces superior wetting on the NiO/YSZ and hence enables the precursor solution to penetrate throughout the substrate. In addition to the uniform distribution and morphology of PdO nanoparticles, the urea decomposition technique with the given molar ratio of urea to cation makes it possible to obtain their crystallization and complete phase formation at the cell operating temperature [34]. Their complete phase formation and chemical compatibility with the NiO/YSZ substrate obtained at 800 °C is evidenced by the XRD analysis which shows that all of the major peaks are identified as PdO, NiO and YSZ, and no secondary phase formation is detected (see Supplementary Fig. S2a).

The PdO nanoparticles uniformly anchored on the backbone structure are subsequently reduced to Pd and alloyed with Ni embedded in the fuel-electrode substrate through the high-temperature metal-oxide reduction process, which satisfies both thermodynamics and diffusion kinetics to form their nanoalloys. After reducing PdO-NiO/YSZ to Pd-Ni/YSZ at 800 °C, it is shown that the reduced Pd nanoparticles are uniformly dispersed on the YSZ grain, but they are hardly seen on the Ni grain, implying their chemical interactions to form Pd-Ni nanoalloys [20]. Gas concentrations were continuously monitored during the metal-oxide reduction process, and no species other than H₂ was detected, indicating that all of the impregnated Pd remains in the fuel-electrode. TEM analysis results, as shown in Fig. 4, indeed elucidate that Pd forms nanoalloys with Ni throughout its grain. It is also confirmed by the XRD analysis obtained after the high-temperature metal-oxide reduction process (see Supplementary Fig. S2b). Thermodynamics indicates that Pd has a solubility for Ni at high temperatures such as those considered in thermo-electrochemical reduction of steam/CO₂, which is a function of time and its diffusivity [35,36]. The presence of Pd on the Ni surface after H₂ reduction treatment at such high-temperature results in their chemical diffusion into the Ni particles and induces *in-situ* nano-alloying. Note that, if the high-temperature metal-oxide reduction process is not properly controlled, PdO may not be fully reduced and left behind, which weakens the effect of nano-alloying. Given the overnight metal-oxide reduction process and volume diffusion of Pd into Ni, the diffusion distance can be calculated by $d = \sqrt{D_{Ni-Pd}t}$, where d is the distance by volume diffusion; D_{Ni-Pd} represents the volume diffusivity of Pd into Ni ($8.01 \times 10^{-18} \text{ m}^2 \text{ s}^{-1}$ at 800 °C) [36]; t is time. The diffusion distance of 0.832 μm is on the order of the size of the Ni grain in the Ni/YSZ substrate. Thus, *in-situ* nano-alloying of Pd nanoparticles with Ni embedded in the substrate satisfies both thermodynamics and diffusion kinetics, which enables complete formation of solid solution during the high-temperature metal-oxide reduction process. Another interesting point evidenced in Fig. 4 is that Pd-Ni nanoalloys are also observed on the YSZ grain after the heat treatment process. Fig. 5 shows that the reduced Pd nanoparticles anchored on the YSZ grain includes Ni atoms, indicating Pd-Ni nanoalloy formation. High-temperature can induce surface diffusion of metal atoms departing from its original grain through the surface of other immiscible species' grains following its chemical concentration gradient. Given the sintered Ni/YSZ fuel-electrode structure in which Ni and YSZ grains are interconnected, Ni atoms diffuse across the surface of the adjacent YSZ grain and coalesce with the Pd nanoparticles impregnated on its grain.

It should be noted that the Pd-Ni nanoalloys are found throughout the Ni grain, attributed to the nano-alloying procedure in a controlled manner. The uniformly-anchored PdO structure and their homogeneous morphology prior to high-temperature metal-oxide reduction makes it possible to obtain such uniform Pd-Ni nanoalloys. The combination of uniform nanoparticle infiltration and *in-situ* nano-alloying techniques enables using substantially

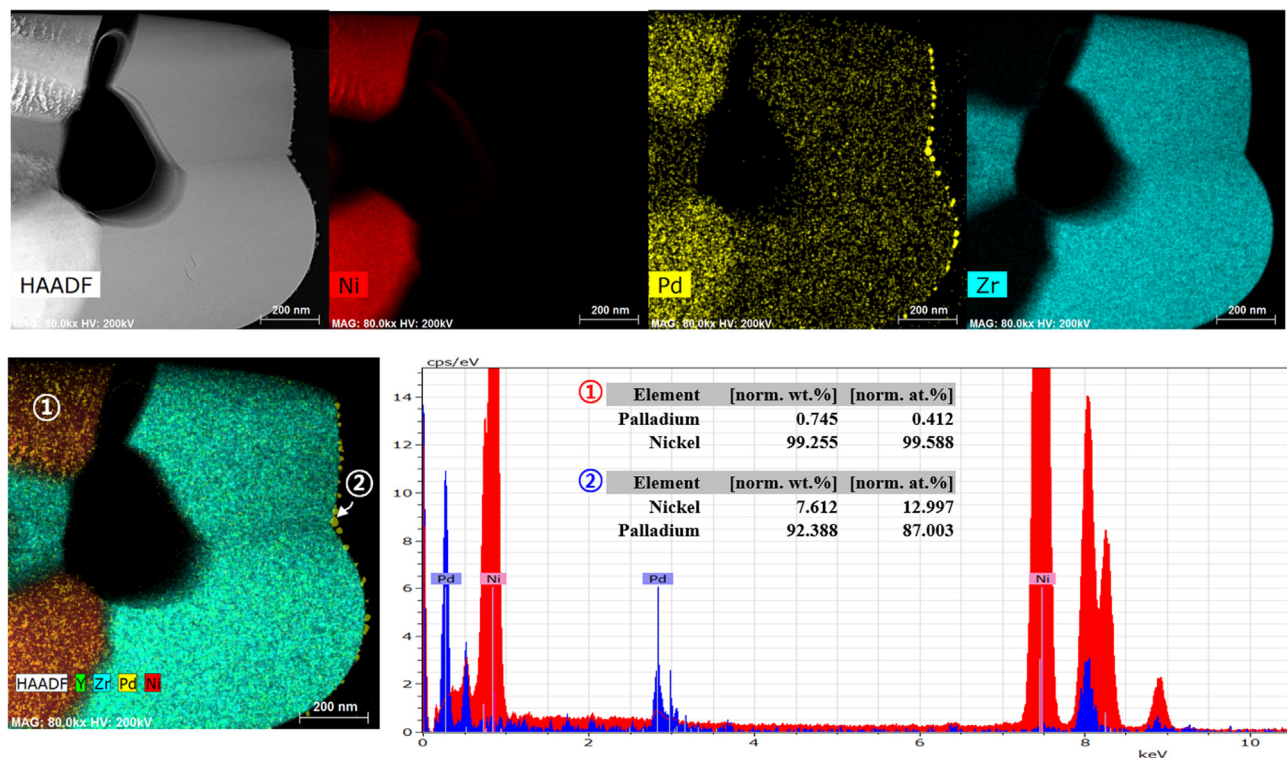


Fig. 4. TEM images with EDS analysis results showing Pd-Ni nanoalloys established in the Ni/YSZ fuel-electrode substrate after the high-temperature metal-oxide reduction process. Compositions of Pd-Ni nanoalloys found in the Ni grain (1) and those observed on the YSZ grain (2) are shown in the lower-right box.

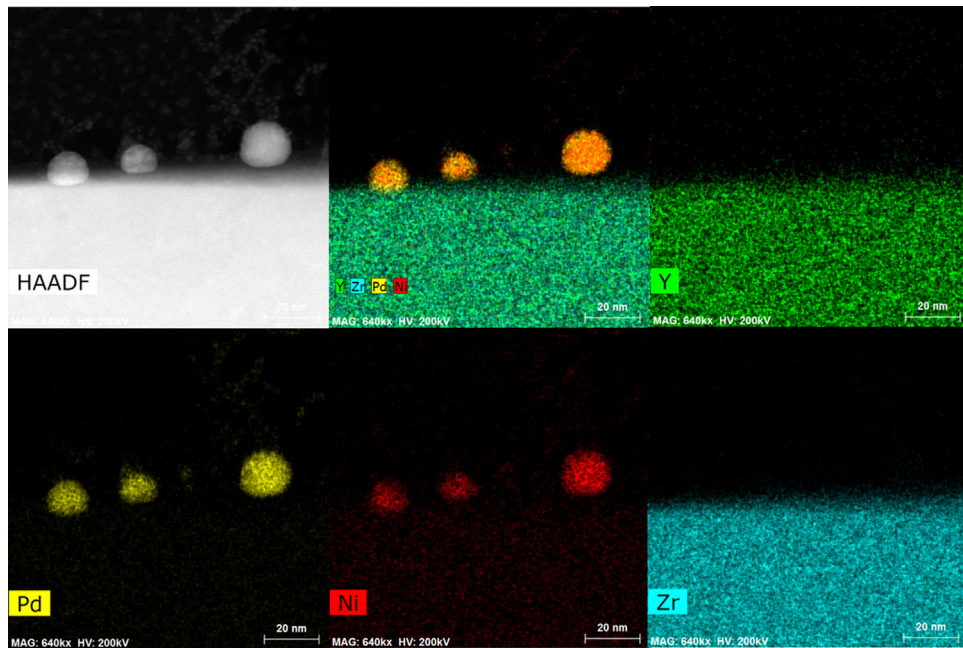


Fig. 5. TEM images with EDS analysis results showing that the nanoparticles found on the YSZ surface are composed of Pd and Ni atoms, elucidating that they are indeed Pd-Ni nanoalloys.

small amount of Pd loadings to form Pd-Ni nanoalloys throughout the fuel-electrode substrate. To fabricate such Pd-Ni nano-alloyed fuel-electrode substrate, only 0.75 mg cm^{-2} of Pd (0.2 wt.%) was used, which is much smaller than loadings considered in typical noble-metal infiltration processes (1–10 wt.%) [37].

3.2. Pd-Ni nanoalloys-assisted control of syngas production

The Pd-Ni nanoalloys improve CO_2 conversion and CO-selectivity by promoting the RWGS reaction. Fig. 6a shows that the CO concentration in the product gas stream of the Pd-Ni nanoalloyed cell is raised in comparison with that of the standard

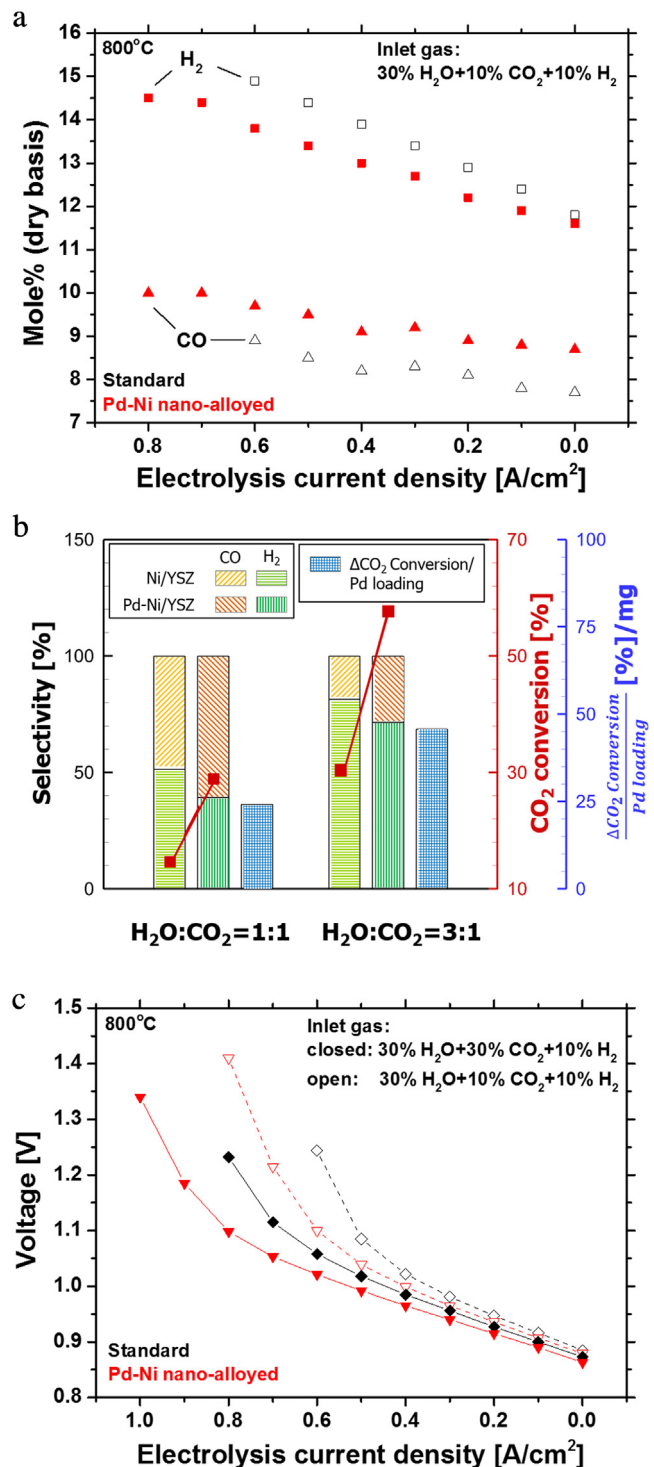


Fig. 6. Catalytic effect of *in-situ* nano-alloyed Pd-Ni on syngas production control and electrochemical cell performance: (a) product gas compositions measured by using Pd-Ni nano-alloyed and standard cells and 30% H₂O/10% CO₂/10% H₂ (with a remainder being argon) as an inlet gas; (b) catalyst powder test results showing the increase in the CO-selectivity (histograms and the value on the left-axis) and CO₂ conversion (red squares and the value on the right-axis) of the Pd-Ni nanoalloys, in comparison with those of Ni, when using 30% H₂O/30% CO₂/10% H₂ (H₂O:CO₂ = 1:1) and 30% H₂O/10% CO₂/10% H₂ (H₂O:CO₂ = 3:1) as inlet gases. The increments of CO₂ conversion per unit Pd loading (the third column of histograms) are also shown on the extended right axis; (c) electrochemical performance of the Pd-Ni nano-alloyed cell as compared to that of the standard cell (for interpretation of the references to colour in this figure legend, the reader is referred to the web version of this article).

(defined as being non-alloyed) cell, while the H₂ concentration is lowered to the same extent. No methane was detected in the product stream, which satisfies thermodynamics of methane formation favored at temperature lower than 650 °C or pressure higher than atmospheric pressure [2]. It can be inferred that the enhanced CO production is attributed to the catalyzed RWGS reaction because the Pd-Ni nanoalloys are established only on the substrate where the thermochemical reactions take place predominantly [38,39], and an increment of the CO concentration is offset by a decrease in the H₂ concentration to the same extent. Higher CO and lower H₂ concentrations at open circuit voltage also supports the reasoning that thermochemical reduction of CO₂ (not electrolysis) accounts for this phenomenon. This argument is verified by complimentary catalysts experiments, in which only thermochemical reactions are assumed, conducted by using the same methodology to prepare Pd-Ni/YSZ powders (0.2 wt.% of Pd included) and considering the same reactant gas compositions as those of the cell test. As shown in Fig. 6b, such nano-alloyed catalyst powders indeed enhance the CO₂ conversion rate and CO production as compared to the standard Ni/YSZ, while decreasing H₂ formation. It can be also observed that the increment in CO₂ conversion per unit Pd loading is substantial. The physics of Pd-Ni nanoalloys' catalytic activity for the RWGS reaction has not been elucidated in details, but previous studies discussed that their electronic modifications may provide distinctive surface sites for the adsorption of reactants, hence promoting subsequent catalytic reactions [22–25]. The density functional theory calculations claim that Pd has a high density of d-electron states on its surface and capability to adsorb a large amount of H₂ atoms [40], which could be enhanced by alloying. The underneath Ni atoms may have an electronic effect on Pd such that the bond strength and Gibbs free energy for electron transfer between Pd and reactants are altered to catalyze heterogeneous reactions [41]. The underlying reaction mechanism of Pd-Ni nanoalloys needs to be examined further in the future research. Furthermore, high CO concentration formed in the fuel-electrode, attributed to the enhanced RWGS reaction by Pd-Ni nanoalloys, may promote carbon formation, which also should be investigated in the following study.

The catalytic effect of Pd-Ni nanoalloys on promoting the RWGS reaction improves the electrochemical cell performance in a way that higher current operation is possible. In syngas production using solid oxide cells, an electrical current level is directly related to their productivity, energy storage capacity and footprints required for system installation. Fig. 6c shows that the concentration polarization of the Pd-Ni nano-alloyed cell plays a role at a higher current density than that of the standard cell, lowering the electrical resistance. The concentration polarization in electrochemical cells is mainly attributed to reactant depletion or its limited transport towards the functional layer. Given the same operating conditions (*i.e.*, same reactant concentrations in the inlet fuel-gas and its temperature) considered for both Pd-Ni nano-alloyed and standard cells, the concentration polarization appearing at a higher current density can be explained by the additional supply of a primary reactant for electrochemical reactions. It was discussed that steam is a primary reactant in electrochemical reactions, and its additional supply during high-temperature cell operation through the RWGS reaction lowers the concentration overpotential [7,13,14]. The Pd-Ni nanoalloys established on the fuel-electrode substrate catalyzes the RWGS reaction to produce additional steam as well as CO and enhances its transport towards the fuel-electrode functional layer where the electrochemical reactions (*i.e.*, H₂O electrolysis) predominantly occur. This corresponds to our previous discussion in which the emergence of concentration polarization was retarded by promoting the kinetics of the RWGS reaction using operating conditions [7]. Therefore, *in-situ* Pd-Ni nano-alloying not only contributes to enhanced syngas pro-

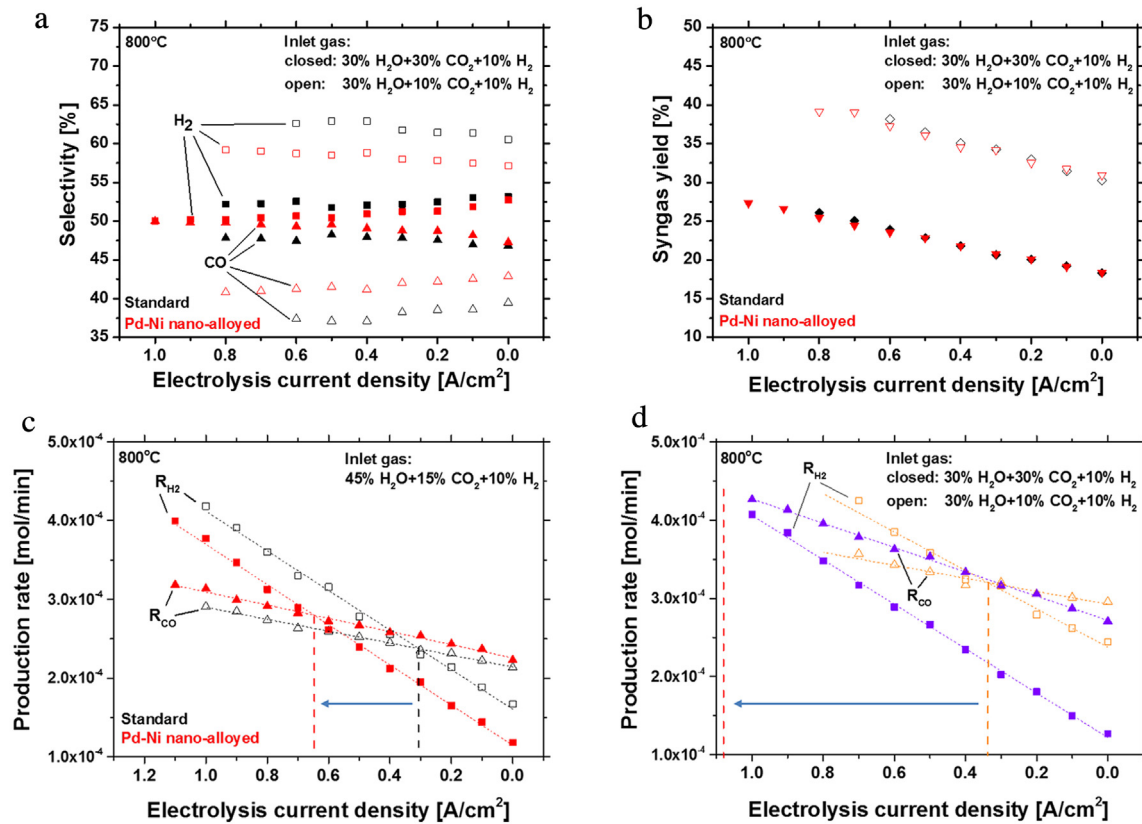


Fig. 7. Pd-Ni nanoalloys-assisted syngas production control. (a) Syngas selectivity, (b) syngas yield, and (c) the molar production rates of CO and H₂, measured from the Pd-Ni nano-alloyed and standard cells; (d) the molar production rates of CO and H₂ measured from the Pd-Ni nano-alloyed cell.

duction by increasing the CO₂ conversion rate, but also improves the electrochemical cell performance by reducing the concentration overpotential. Note that the syngas yield increases with raising the current density, and thermo-electrochemical reactions taking place on the fuel-electrode are highly endothermic. Pd-Ni nanoalloys' effect on the electrochemical cell performance can extend operating conditions to a higher current density while lowering an overvoltage, which enables obtaining higher system efficiency and lower energy requirements.

Given Pd-Ni nanoalloys' catalytic activity, they indeed increase the CO-selectivity while preserving the syngas production yield (defined elsewhere [7]), as shown in Fig. 7a and b. The syngas production yield determines the high-temperature thermo-electrochemical steam/CO₂ reduction system efficiency, while its selectivity influences syngas post-processing such as the Fischer-Tropsch process via the H₂/CO molar ratio of the product gas and hence the type of synthetic hydrocarbon fuels. Therefore, employing the Pd-Ni nanoalloys in the fuel-electrode of solid oxide cells can formulate synthetic fuels which include higher carbon contents without sacrificing their energy storage efficiency. Given the H₂/CO molar ratio ranging from 1.0 to 1.6 obtained in this study, the final products may encompass methanol, ethanol, dimethyl ether (DME) and diesel. It should be noted that the syngas selectivity is predominantly determined by the extent of each reaction throughout the current density. The syngas selectivity shown in Fig. 7a does not change to a large extent with raising the current density, as compared to the syngas yield shown in Fig. 7b. Instead, the selectivity was varied largely by nano-alloying Pd-Ni that changes the reaction kinetics in the fuel-electrode. It was discussed that the syngas selectivity is also dependent on operating conditions such as fuel-gas compositions which influence the chemical kinetics of the thermo-electrochemical reactions taking place in the fuel-electrode [7].

Given the fact that the syngas selectivity is primarily determined by the chemical reaction kinetics, controlling the kinetics and thus the extent of each reaction through employing the Pd-Ni nanoalloys can effectively change the syngas quality. Since the primary goals of high-temperature thermo-electrochemical reduction of steam/CO₂ include syngas production with desirable gas compositions required for post-processing, obtaining the capability to control the syngas selectivity is essential. In this regard, along with changing operating conditions, fabricating Pd-Ni nanoalloys uniformly throughout the fuel-electrode substrate is a promising technique to control the syngas quality.

In addition to increasing the CO₂ conversion rate, enabling higher current operation and controlling the syngas selectivity, the Pd-Ni nanoalloys can change the applied current density required for desirable syngas production. Fig. 7c shows the production rates of H₂ and CO from the Pd-Ni nano-alloyed and standard cells. It can be seen that the intersection between these rates is obtained at different current densities for the two cells. Although the overall reaction scheme is largely determined by the chemical reaction kinetics according to given inlet fuel-gas conditions, micro-managing the reaction regime during operation may be needed by varying an applied current density. In this case, the Pd-Ni nanoalloys can change the current density at which the H₂ production rate exceeds that of CO formation or vice versa. This in turn influences the operating current density of high-temperature thermo-electrochemical reduction of steam/CO₂ at various inlet fuel-gas conditions, as shown in Fig. 7d. The operating current density would play a critical role in determining the effectiveness of these cells when combined with renewable energy sources. As evidenced in the results, *in-situ* nano-alloying Pd-Ni modifies the electrical current level required for the production rates of H₂ and CO and subsequently affects the operating conditions of high-

temperature thermo-electrochemical reduction of steam/CO₂. The development of the nano-structured fuel-electrode by *in-situ* nano-alloying Pd-Ni can be an effective technique to manipulate the operating current density needed for desirable syngas production, enabling versatile operations when these cells are coupled with renewable energy and CO₂ sources.

In-situ nano-alloying Pd-Ni in the fuel-electrode substrate enables controlling syngas production from high-temperature thermo-electrochemical reduction of steam/CO₂ mixtures by using substantially small amount of Pd loadings. Given the twice larger CO₂ conversion rate of the Pd-Ni nanoalloys sample (*i.e.*, given the molar ratio of H₂O to CO₂ at one and three, the CO₂ conversion rates are 28.8% and 57.7% for Pd-Ni/YSZ and 14.3% and 30.3% for Ni/YSZ, respectively), it can be argued that the chemical kinetics for enhancing CO₂ conversion and CO-selectivity is enhanced by a factor of two. Their effectiveness for controlling syngas production is more evident when considering the increment of CO₂ conversion per unit Pd loading used (*i.e.*, given the molar ratio of H₂O to CO₂ at one and three, the increments are 24.2%/mg and 45.7%/mg, respectively) and the long-term stability for high-temperature operations (see Supplementary Fig. S3). Considering that such small loadings of the noble metal-catalyst result in substantial increment of the CO₂ conversion, it can be concluded that Pd-Ni nanoalloys-assisted control of syngas production is an economical technique.

4. Conclusions

A novel methodology for *in-situ* nano-alloying Pd-Ni was proposed to enhance the feasibility of synthetic gas production from high-temperature thermo-electrochemical reduction of steam/CO₂ mixtures. Two consecutive processes comprised of uniform nanoparticle infiltration and high-temperature metal-oxide reduction result in homogeneous distribution and morphology of *in-situ* nano-alloyed Pd-Ni. With an aid of the nano-alloying procedure in a controlled manner, Pd-Ni nanoalloys were observed throughout the backbone structure by using only 0.75 mg cm⁻² of Pd (0.2 wt%). Such Pd-Ni nanoalloys were established only in the fuel-electrode substrate of solid oxide cells where thermochemical reactions proceed dominantly, hence catalyzing selectively the reverse water gas shift reaction. This increases the CO₂ conversion rate and CO-selectivity, providing a large increment of CO₂ conversion per unit Pd loading used such as 24.2–45.7%/mg. In addition, the catalytic effect of the Pd-Ni nanoalloys on the electrochemical cell performance can extend operating conditions to a higher current density while lowering an overvoltage, which enables obtaining higher energy storage capacity and syngas productivity. When this system is linked with renewable energy and CO₂ sources, the proposed methodology provides a capability for adjusting effectively the high-temperature thermo-electrochemical steam/CO₂ reduction system to their fluctuating electrical current and gas flow rates.

Acknowledgments

This work was supported by the New & Renewable Energy Core Technology Program of the Korea Institute of Energy Technology Evaluation and Planning (KETEP) granted financial resource from the Ministry of Trade, Industry & Energy, Republic of Korea (No. 20143030031430) and partially supported by the Institutional Research Program of the Korea Institute of Science and Technology (2E26081).

Appendix A. Supplementary data

Supplementary data associated with this article can be found, in the online version, at <http://dx.doi.org/10.1016/j.apcatb.2016.07.008>.

References

- [1] C. Graves, S.D. Ebbesen, M. Mogensen, K.S. Lackner, Sustainable hydrocarbon fuels by recycling CO₂ and H₂O with renewable or nuclear energy, *Renew. Sustainable Energy Rev.* 15 (2011) 1–23.
- [2] D.M. Bierschenk, J.R. Wilson, S.A. Barnett, High efficiency electrical energy storage using a methane-oxygen solid oxide cell, *Energy Environ. Sci.* 4 (2011) 944–951.
- [3] Q. Fu, C. Mabilat, M. Zahid, A. Brisse, L. Gautier, Syngas production via high-temperature steam/CO₂ co-electrolysis: an economic assessment, *Energy Environ. Sci.* 3 (2010) 1382–1397.
- [4] J.E. O'Brien, M.G. McKellar, E.A. Harvego, C.M. Stoops, High-temperature electrolysis for large-scale hydrogen and syngas production from nuclear energy – summary of system simulation and economic analyses, *Int. J. Hydrogen Energy* 35 (2010) 4808–4819.
- [5] L. Chen, F. Chen, C. Xia, Direct synthesis of methane from CO₂-H₂O co-electrolysis in tubular solid oxide electrolysis cells, *Energy Environ. Sci.* 7 (2014) 4018–4022.
- [6] C. Yang, J. Li, J. Newkirk, V. Baish, R. Hu, Y. Chen, F. Chen, Co-electrolysis of H₂O and CO₂ in a solid oxide electrolysis cell with hierarchically structured porous electrodes, *J. Mater. Chem. A* 3 (2015) 15913–15919.
- [7] S.-W. Kim, H. Kim, K.J. Yoon, J.-H. Lee, B.-K. Kim, W. Choi, J.-H. Lee, J. Hong, Reactions and mass transport in high temperature co-electrolysis of steam/CO₂ mixtures for syngas production, *J. Power Sources* 280 (2015) 630–639.
- [8] C. Graves, S.D. Ebbesen, S.H. Jensen, S.B. Simonsen, M.B. Mogensen, Eliminating degradation in solid oxide electrochemical cells by reversible operation, *Nat. Mater.* 14 (2015) 239–244.
- [9] S.D. Ebbesen, R. Knibbe, M. Mogensen, Co-electrolysis of steam and carbon dioxide in solid oxide cells, *J. Electrochem. Soc.* 159 (2012) F482–F489.
- [10] C. Graves, S.D. Ebbesen, M. Mogensen, Co-electrolysis of CO₂ and H₂O in solid oxide cells: performance and durability, *Solid State Ionics* 192 (2011) 398–403.
- [11] S.D. Ebbesen, J. Høgh, K.A. Nielsen, J.U. Nielsen, M. Mogensen, Durable SOC stacks for production of hydrogen and synthesis gas by high temperature electrolysis, *Int. J. Hydrogen Energy* 36 (2011) 7363–7373.
- [12] S.H. Jensen, X. Sun, S.D. Ebbesen, R. Knibbe, M. Mogensen, Hydrogen and synthetic fuel production using pressurized solid oxide electrolysis cells, *Int. J. Hydrogen Energy* 35 (2010) 9544–9549.
- [13] C.M. Stoops, J.E. O'Brien, J.S. Herring, J.J. Hartvigsen, Syngas production via high-temperature coelectrolysis of steam and carbon dioxide, *J. Fuel Cell Sci. Technol.* 6 (2009).
- [14] C. Stoops, J. O'Brien, J. Hartvigsen, Results of recent high temperature coelectrolysis studies at the Idaho National Laboratory, *Int. J. Hydrogen Energy* 34 (2009) 4208–4215.
- [15] T. Takeuchi, R. Kikuchi, T. Yano, K. Eguchi, K. Murata, Effect of precious metal addition to Ni-YSZ cermet on reforming of CH₄ and electrochemical activity as SOFC anode, *Catal. Today* 84 (2003) 217–222.
- [16] G. Pekridis, K. Kalimeri, N. Kaklidis, E. Vakouftsi, E.F. Iliopoulos, C. Athanasiou, G.E. Marnellos, Study of the reverse water gas shift (RWGS) reaction over Pt in a solid oxide fuel cell (SOFC) operating under open and closed-circuit conditions, *Catal. Today* 127 (2007) 337–346.
- [17] S.P. Jiang, Y. Ye, T. He, S.B. Ho, Nanostructured palladium-La_{0.75}Sr_{0.25}Cr_{0.5}Mn_{0.5}O₃/V2O₃-ZrO₂ composite anodes for direct methane and ethanol solid oxide fuel cells, *J. Power Sources* 185 (2008) 179–182.
- [18] H.P. He, A. Wood, D. Steedman, M. Tilleman, Sulphur tolerant shift reaction catalysts for nickel-based SOFC anode, *Solid State Ionics* 179 (2008) 1478–1482.
- [19] M.D. Gross, J.M. Vohs, R.J. Gorte, An examination of SOFC anode functional layers based on ceria in YSZ, *J. Electrochem. Soc.* 154 (2007) B694–B699.
- [20] Y. Nabae, I. Yamanaka, M. Hatano, K. Otsuka, Catalytic behavior of Pd-Ni/composite anode for direct oxidation of methane in SOFCs, *J. Electrochem. Soc.* 153 (2006) A140–A145.
- [21] Y. Nabae, I. Yamanaka, M. Hatano, K. Otsuka, Mechanism of suppression of carbon deposition on the Pd-Ni/Ce(Sm)O₂-La(Sr)CrO₃ anode in dry CH₄ fuel, *J. Phys. Chem. C* 112 (2008) 10308–10315.
- [22] L. Chen, H. Guo, T. Fujita, A. Hirata, W. Zhang, A. Inoue, M. Chen, Nanoporous PdNi bimetallic catalyst with enhanced electrocatalytic performances for electro-oxidation and oxygen reduction reactions, *Adv. Funct. Mater.* 21 (2011) 4364–4370.
- [23] B. Coq, F. Figueras, Bimetallic palladium catalysts: influence of the co-metal on the catalyst performance, *J. Mol. Catal. A: Chem.* 173 (2001) 117–134.
- [24] Y. Mukainakano, B. Li, S. Kado, T. Miyazawa, K. Okumura, T. Miyao, S. Naito, K. Kunimori, K. Tomishige, Surface modification of Ni catalysts with trace Pd and Rh for oxidative steam reforming of methane, *Appl. Cata. A: Gen.* 318 (2007) 252–264.

- [25] P. Hermann, J.M. Guigner, B. Tardy, Y. Jugnet, D. Simon, J.C. Bertolini, The Pd/Ni(110) bimetallic system: surface characterisation by LEED, AES, XPS, and LEIS techniques; new insight on catalytic properties, *J. Catal.* 163 (1996) 169–175.
- [26] Y.A. Daza, J.N. Kuhn, CO₂ conversion by reverse water gas shift catalysis: comparison of catalysts, mechanisms and their consequences for CO₂ conversion to liquid fuels, *RSC Adv.* 6 (2016) 49675–49705.
- [27] J. Ko, B.-K. Kim, J.W. Han, Density functional theory study for catalytic activation and dissociation of CO₂ on bimetallic alloy surfaces, *J. Phys. Chem. C* 120 (2016) 3438–3447.
- [28] S.I. Lee, J. Kim, J.W. Son, J.H. Lee, B.K. Kim, H.J. Je, H.W. Lee, H. Song, K.J. Yoon, High performance air electrode for solid oxide regenerative fuel cells fabricated by infiltration of nano-catalysts, *J. Power Sources* 250 (2014) 15–20.
- [29] J.-H. Lee, H. Kim, S.M. Kim, T.-W. Noh, H.-Y. Jung, H.-Y. Lim, H.-G. Jung, J.-W. Son, H.-R. Kim, B.-K. Kim, H.-J. Je, J.-C. Lee, H. Song, H.-W. Lee, Effect of elastic network of ceramic fillers on thermal cycle stability of a solid oxide fuel cell stack, *Adv. Energy Mater.* 2 (2012) 461–468.
- [30] S.P. Jiang, Nanoscale and nano-structured electrodes of solid oxide fuel cells by infiltration: advances and challenges, *Int. J. Hydrogen Energy* 37 (2012) 449–470.
- [31] S. Jung, C. Lu, H. He, K. Ahn, R.J. Gorte, J.M. Vohs, Influence of composition and Cu impregnation method on the performance of Cu/CeO₂/YSZ SOFC anodes, *J. Power Sources* 154 (2006) 42–50.
- [32] A. Babaei, S.P. Jiang, J. Li, Electrocatalytic promotion of palladium nanoparticles on hydrogen oxidation on Ni/GDC anodes of SOFCs via spillover, *J. Electrochim. Soc.* 156 (2009) B1022–B1029.
- [33] W.Y. Li, Z. Lu, X.B. Zhu, B. Guan, B. Wei, C.Z. Guan, W.H. Su, Effect of adding urea on performance of Cu/CeO₂/yttria-stabilized zirconia anodes for solid oxide fuel cells prepared by impregnation method, *Electrochim. Acta* 56 (2011) 2230–2236.
- [34] D. Sordelet, M. Akinc, Preparation of spherical, monosized Y₂O₃ precursor particles, *J. Colloid Interface Sci.* 122 (1988) 47–59.
- [35] L.E. Murr, *Interfacial Phenomena in Metals and Alloys*, Addison-Wesley Publishing Co., Reading, Massachusetts, 1975.
- [36] G. Ghosh, C. Kanter, G.B. Olson, Thermodynamic modeling of the Pd-X (X = Ag, Co Fe, Ni) systems, *JPE* 20 (1999) 295–308.
- [37] J.T.S. Irvine, D. Neagu, M.C. Verbraeken, C. Chatzichristodoulou, C. Graves, M.B. Mogensen, Evolution of the electrochemical interface in high-temperature fuel cells and electrolyzers, *Nat. Energy* 1 (2016) 15014.
- [38] J. Hanna, W.Y. Lee, Y. Shi, A.F. Ghoniem, Fundamentals of electro- and thermochemistry in the anode of solid-oxide fuel cells with hydrocarbon and syngas fuels, *Prog. Energy Combust. Sci.* 40 (2014) 74–111.
- [39] S. Lee, H. Kim, K.J. Yoon, J.-W. Son, J.-H. Lee, B.-K. Kim, W. Choi, J. Hong, The effect of fuel utilization on heat and mass transfer within solid oxide fuel cells examined by three-dimensional numerical simulations, *Int. J. Heat Mass Transfer* 97 (2016) 77–93.
- [40] B. Hammer, J.K. Nørskov, Theoretical surface science and catalysis—calculations and concepts, in: *Advances in Catalysis*, Academic Press, 2000, pp. 71–129.
- [41] J.X. Wang, N.M. Markovic, R.R. Adzic, Kinetic analysis of oxygen reduction on Pt(111) in acid solutions: intrinsic kinetic parameters and anion adsorption effects, *J. Phys. Chem. B* 108 (2004) 4127–4133.